UILU-ENG-2000-2802

OPERATING EFFICIENCY OPTIMIZATION OF A FIELD-ORIENTED-CONTROLLED INDUCTION MACHINE

DANIEL LOGUE
PHILIP KREIN

CEME-TR-00-2
September 2000

Grainger Center for Electric Machinery and Electromechanics
Department of Electrical and Computer Engineering
University of Illinois at Urbana/Champaign
Urbana, Illinois 61801

Abstract

Ripple correlation control makes use of the inherent switching ripple in a power converter to minimize or maximize input power. This report develops a complete analytical and simulation model of an induction motor drive system, with ripple correlation control used for efficiency optimization. The analysis utilizes a Matlab model for field-oriented control (FOC) of a three-phase induction machine. The FOC method analyzed here is indirect: it operates with a flux observer derived from rotor position and stator current information. The algorithm includes an observer to correct for variations in the rotor time constant. The analysis incorporates a saturation function to model nonlinear magnetics. FOC is used to control a pulse-width modulated (PWM) inverter. The inverter input dc bus is obtained from a six-pulse rectifier. Ripple on the dc bus is applied to ripple correlation control, which is used to alter the motor operating flux. It is well known that motor efficiency is best at a particular flux value that depends on the operating point. With the control introduced here, the flux is adjusted dynamically to drive the system to its best efficiency under all conditions. The algorithm employs a parameter observer to correct for inductive effects in the motor windings.

Conventional electric machines are designed to have maximum efficiency at rated load and rated flux. In induction motors, efficiency can be improved under light-load conditions by reducing the operating flux. Optimal flux adjustment allows the efficiency to be nearly constant with load – at the highest attainable value. (For instance, a motor with a tested peak efficiency of 90% can operate with an efficiency of about 90% across its full range of loads with optimal flux adjustment.) Simulation studies are presented in the case in which ripple correlation control is used to adjust for optimal flux. A sample

motor, with peak efficiency under conventional conditions of about 66%, is used to illustrate the possible results. The optimizing control is designed to work slowly, without interfering with the dynamics of FOC. The design presented here operates on time scales of about 30 s, working in the background while the complete FOC system functions. Operation is illustrated for step changes in both the commanded motor speed and the applied shaft torque. For this sample motor, efficiencies of 66% or better are obtained over the full rated load range, as compared to much lower efficiencies (less than 20% at 20% load) obtained without optimal flux adjustment. The results demonstrate that ripple correlation control can be used to augment even very sophisticated motor controllers, and that it supports efficiency maximization without interfering with dynamic performance. Considerable energy savings can be obtained in cases in which a motor is often used below its rated load condition.

CONTENTS

LIST OF TABLES

LIST OF FIGURES

1 Introduction

Ripple correlation control, first proposed in the context of solar power conversion [1,2], is uniquely suited to optimization problems encountered in power electronics [3]. In this control approach, the ripple inherent in a switching power converter is used as an *internal perturbation* for a control method. The general possibilities are similar to those of vibratory control [4], except that no external vibration needs to be imposed.

The classic solar power conversion problem, maximum power point tracking (MPPT) is to draw power from a solar array at the highest possible value. The best conventional approach, termed *perturb and observe* [5,6], alters a switching converter's duty ratio, exploring parameter values until the highest power is attained. Since panel conditions change over time, the process must continue indefinitely.

With ripple correlation, the converter ripple itself is interpreted as a perturbation. In place of a measurement, a cross-correlation between power ripple and the switching signal shows when the converter operation straddles the maximum power point. An integral controller will drive the converter to the maximum power point [1]. A typical perturb-and-observe process works on time scales of seconds, while ripple correlation works on the millisecond time scales of switching functions.

There is a question that arises when applying ripple correlation to solar power conversion on fast time scales (1ms and below): does the ripple in fact represent a perturbation in panel power? A real solar panel has substantial parallel capacitance, so the answer is not obvious. In practical solar configurations, this question has a useful answer.

Ripple voltage produces both a perturbation on panel current and a current that flows in the panel capacitance. A panel large enough to supply 3A at about 12V will have capacitance that does not exceed 0.1μF. At 10kHz with 2% ripple the expected capacitive current is less than 0.25mA. The 2% ripple would imply current ripple on the order of 60mA --- orders of magnitude larger. Furthermore, the capacitive current has an orthogonal relation with the power-generating current. If the value of capacitance is known, it is possible to compensate for this effect.

Ripple correlation control has also been proposed for power tracking in motor applications [2]. The problem in many ways is the dual of the solar power problem, since a motor has series inductance and most likely minimum power is of interest. The application of ripple correlation control to the problem of motor power minimization is one of great practical interest. This is especially important as electronic motor drive applications expand.

It is well known that motor efficiency depends on the excitation flux, and that for any given operating condition, there is a specific flux value that will minimize power consumption [7]. In principle, a perturb-and-observe technique can be applied to this problem: flux value is altered slightly, subject to the speed and torque requirements of the load, and power can be measured. The flux again can be altered and a decision is then made whether the new value is better or worse. This would continue indefinitely.

On the other hand, a switching motor drive system is the most convenient way to adjust speed, torque, and power. If switching takes place, ripple will be present and presumably ripple correlation control can be applied. Since motor windings are inductive, the question arises whether a perturbation influences power or just the inductor voltage.

Unlike the solar power case, the answer in the context of a motor is that inductor drop cannot be neglected. If ripple alone is used for control, minimum power will not be reached.

As in the solar power case, it is possible to compensate for inductance. If winding inductance L_w is known, a correction term L_w *di/dt* can be subtracted from the ripple voltage to give a "true" representation of the ripple power. This signal then functions in a ripple correlation control. Of course, in general the inductor value is unknown. It must either be measured or obtained with an observer or other similar active method.

This paper describes the use of ripple correlation control in a conventional ac induction motor operating from a high-performance field-oriented control (FOC) system. In such a system, a pulse-width modulated (PWM) inverter powers the motor. Both flux and torque are controlled independently. In conventional applications flux is set to its rated value. With ripple correlation, flux is driven dynamically to the value that minimizes input electrical power.

2 Overview

We report in detail the modeling and simulation of an FOC machine drive and demonstrate the magnitude of system efficiency gain as a function of decrease in motor load below design maximum or optimum. For ease of simulation the induction machine is modeled in the synchronous reference frame. The FOC method utilized is indirect: the rotor position and stator currents provide the necessary information for rotor flux alignment. The drive is supplied by a six-pulse rectifier with LC output filter.

The control method also addresses the variation of the rotor LR time constant due to temperature changes. A parameter estimator based on measurement of the rotor flux alignment is used to provide this time constant for use by the FOC controller.

Maximum operating efficiency is achieved via a maximum power-point tracker (MPPT). The MPPT adjusts the rotor flux to achieve maximum efficiency. It does so by using information about the correlation between the change in the inverter dc bus power and the change in rotor flux while the system is being perturbed repetitively. The perturbations in input power and rotor flux are not artificially introduced, rather induced by the ripple content of the front-end rectifier supplying the dc bus. The input power is readily available, but the rotor flux, not being directly accessible, must be calculated. It is easily achieved in a reference frame attached to the rotor. Note that this calculation requires the rotor LR time constant provided by the parameter estimator described above. Modeling of the listed systems will be presented first, followed by simulation results for various operating conditions.

3 System Modeling

Figure 1 shows the block diagram of the complete maximum efficiency motor control system. Modeling of the induction machine, FOC drive, front-end rectifier, and MPPT are described. The methods of calculation of the rotor flux and estimation of the rotor time constant are also provided. A nomenclature is presented in Table 1.

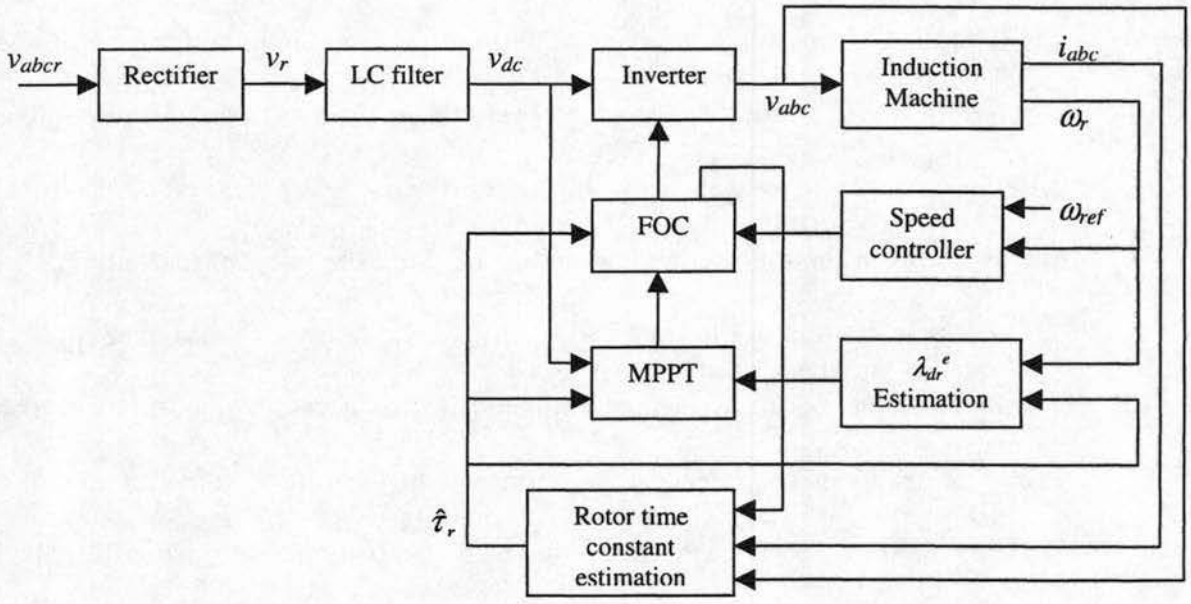

Figure 1: Complete maximum efficiency motor control system

Table 1: Nomenclature.

Symbol	Description
p	Derivative operator
ψ_{qs}^{e}	Stator q-axis flux linkage-per-second (Synchronous frame)
ψ_{ds}^{e}	Stator d-axis flux linkage-per-second (Synchronous frame)
ψ_{qr}^{e}	Rotor q-axis flux linkage-per-second (Synchronous frame)
ψ_{dr}^{e}	Rotor d-axis flux linkage-per-second (Synchronous frame)
ω_b	Machine base frequency (rad/s)
ω_r	Machine shaft speed (electrical rad/s)
ω_e	Synchronous speed (rad/s)
θ_e	Angle between stationary and synchronous frames
T_e	Developed electrical shaft torque
P	Number of machine poles
v_{qs}^{e}	Induction machine q-axis stator voltage
v_{ds}^{e}	Induction machine d-axis stator voltage
i_{qs}^{e}	Induction machine q-axis stator current
i_{ds}^{e}	Induction machine d-axis stator current
i_{qr}^{e}	Induction machine q-axis rotor current
i_{dr}^{e}	Induction machine d-axis rotor current
r_s	Stator series resistance
r_r	Referred rotor resistance
X_{ls}	Stator leakage reactance
X_{lr}	Referred rotor leakage reactance

3.1 Induction Machine Modeling in the Synchronous Reference Frame

The induction machine is modeled with stator and rotor flux-linkages-per-second as states [8-9]. These quantities are related to the flux linkages by the base speed as $\psi_i = \omega_b \lambda_i$. Symmetrical operation of the induction machine is assumed hence, the zero sequence states are not needed. Equations (1)-(8) model the induction machine.

$$\frac{d\psi^e_{qs}}{dt} = \omega_b \left[v^e_{qs} - \frac{\omega_e}{\omega_b}\psi^e_{ds} + \frac{r_s}{X_{ls}}\left(\psi_{mq} - \psi^e_{qs}\right)\right] \tag{1}$$

$$\frac{d\psi^e_{ds}}{dt} = \omega_b \left[v^e_{ds} + \frac{\omega_e}{\omega_b}\psi^e_{qs} + \frac{r_s}{X_{ls}}\left(\psi_{md} - \psi^e_{ds}\right)\right] \tag{2}$$

$$\frac{d\psi^{e\prime}_{qr}}{dt} = \omega_b \left[-\frac{\omega_e - \omega_r}{\omega_b}\psi^{e\prime}_{dr} + \frac{r_r'}{X_{lr}'}\left(\psi_{mq} - \psi^{e\prime}_{qr}\right)\right] \tag{3}$$

$$\frac{d\psi^{e\prime}_{dr}}{dt} = \omega_b \left[\frac{\omega_e - \omega_r}{\omega_b}\psi^{e\prime}_{qr} + \frac{r_r'}{X_{lr}'}\left(\psi_{md} - \psi^{e\prime}_{dr}\right)\right] \tag{4}$$

The quantities v^e_{qs} and v^e_{ds} are the stator input voltages in *dq* coordinates. Here, the superscript 'e' represents the synchronously rotating reference frame and the primes indicate referred rotor quantities. The quantities X_{ls} and X_{lr}' are the stator and rotor leakage reactances, respectively. The stator and rotor series resistances are r_s and r_r', respectively. The quantities ω_e and ω_r denote the speed of the synchronous and rotor

reference frames in electrical radians-per-second, respectively. The flux linkages-per-second ψ_{mq} and ψ_{md} are given by

$$\psi_{mq} = X_a\left(\frac{\psi^e_{qs}}{X_{ls}} + \frac{\psi^{e\prime}_{qr}}{X'_{lr}}\right) - \frac{X_a}{X_M} f_{sat}\left(\psi_{mq}, \psi_{md}\right) \tag{5}$$

$$\psi_{md} = X_a\left(\frac{\psi^e_{ds}}{X_{ls}} + \frac{\psi^{e\prime}_{dr}}{X'_{lr}}\right) - \frac{X_a}{X_M} f\left(\psi_{mq}, \psi_{md}\right) \tag{6}$$

where X_M is the magnetizing reactance of the machine, and X_a is defined by

$$X_a = \left(\frac{1}{X_M} + \frac{1}{X_{ls}} + \frac{1}{X'_{lr}}\right)^{-1}$$

The electrical shaft torque of the machine is given by

$$T_e = \frac{3P}{4}\left(\lambda^e_{ds} i^e_{qs} - \lambda^e_{qs} i^e_{ds}\right) \tag{7}$$

and the shaft speed is governed by

$$\frac{d\omega_{rm}}{dt}\frac{1}{J}\left(T_e - T_{load}\right) \tag{8}$$

where J is the rotational inertia constant of the machine and ω_r is in mechanical radians-per-second. The quantities ω_r and ω_{rm} are related as follows:

$$\omega_r = \frac{P}{2}\omega_{rm} \tag{9}$$

The function $f_{sat}(\cdot)$ in (5) and (6) is used to facilitate the modeling of magnetic saturation. This correction term is a function of the quantity $\sqrt{\psi_{mq}^2 + \psi_{md}^2}$. Saturation of the machine is one reason that (7) was chosen for calculation of the developed shaft torque. This particular form for the shaft toque does not involve X_M, which is not constant under the effects of saturation [8]. The stator input currents in *dq* coordinates are

$$i_{qs}^e = \frac{1}{X_{ls}}\left(\psi_{qs}^e - \psi_{mq}\right) \tag{10}$$

$$i_{ds}^e = \frac{1}{X_{ls}}\left(\psi_{ds}^e - \psi_{md}\right) \tag{11}$$

In order to effectively interface the machine to the front-end rectifier, the machine variables must be placed in stationary *abc* coordinates. This is done by multiplying the vector of *dq0* components by K_s^{-1} to convert from the synchronous *dq0* to the *abc* coordinate frame as shown in (12). It is understood that the reverse is also possible by multiplying the *abc* components by K_s.

$$f_{abc}^s = K_s^{-1} f_{dq0}^e \tag{12}$$

where

$$f_{abc} = \begin{bmatrix} f_a & f_b & f_c \end{bmatrix}^T$$
$$f_{dq0} = \begin{bmatrix} f_d & f_q & f_0 \end{bmatrix}^T$$

can be any be any set of variables associated with the machine. The matrices K_s and K_s^{-1} are given by (13) and (14), respectively.

$$K_s = \frac{2}{3}\begin{bmatrix} \cos(\theta_e) & \cos(\theta_e - \frac{2\pi}{3}) & \cos(\theta_e + \frac{2\pi}{3}) \\ \sin(\theta_e) & \sin(\theta_e - \frac{2\pi}{3}) & \sin(\theta_e + \frac{2\pi}{3}) \\ \frac{1}{2} & \frac{1}{2} & \frac{1}{2} \end{bmatrix} \tag{13}$$

$$K_s^{-1} = \begin{bmatrix} \cos(\theta_e) & \sin(\theta_e) & 1 \\ \cos(\theta_e - \frac{2\pi}{3}) & \sin(\theta_e - \frac{2\pi}{3}) & 1 \\ \cos(\theta_e + \frac{2\pi}{3}) & \sin(\theta_e + \frac{2\pi}{3}) & 1 \end{bmatrix} \tag{14}$$

where

$$\theta_e = \int_0^t \omega_e dt$$

The induction machine top-level SIMULINK block diagram is shown in Figure 2. The stator block incorporates (1) and (2), the rotor block contains (3) and (4), the Phi_m block contains (5) and (6), and the mechanical dynamics block uses equations (7)-(11).

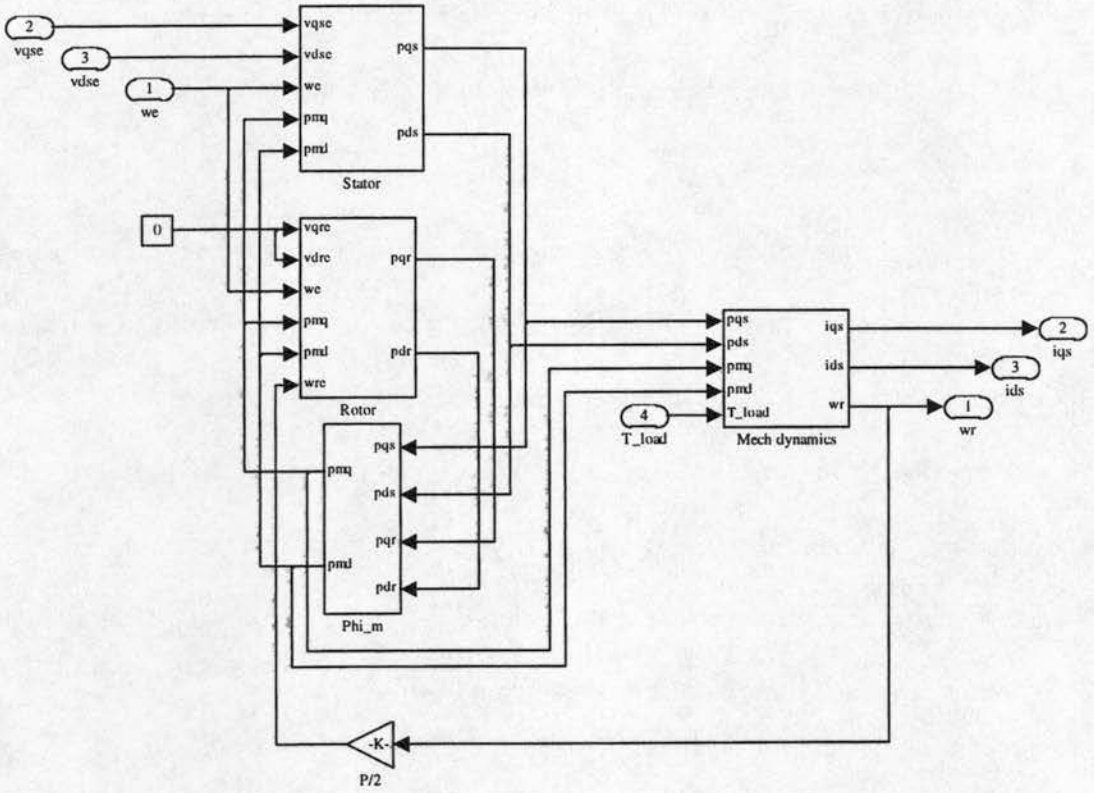

Figure 2: Induction machine top-level SIMULINK block diagram.

3.2 Front-end Rectifier Modeling

The rectifier is a three-phase diode bridge followed by a LC filter. It is assumed that the rectifier operates in continuous conduction mode [10]. This is justified if the filter inductance and capacitance are chosen properly and the motor is loaded. This being the case, the filter input voltage is easily calculated as

$$v_r = \max(v_{ar}, v_{br}, v_{cr}) - \min(v_{ar}, v_{br}, v_{cr})$$

where the rectifier input voltages v_{ar}, v_{br}, and v_{cr} form a three-phase balanced set. The rectifier output voltage ripple therefore contains a first harmonic at six times the rectifier input frequency.

The motor reference voltages are generated by the FOC controller and supplied to a pulse-width-modulated (PWM) inverter. The necessary phase voltages are then created by the inverter. In order to mimic the real system, the rectifier ripple must be imposed on these voltages in some manner. A two-level PWM drive generates three modulating functions, call them $d_1(t)$, $d_2(t)$, and $d_3(t)$, from which the machine voltages v_a, v_b, and v_c are constructed. These functions define duty ratio of the corresponding switches in the inverter. The modulating functions are given by

$$\begin{aligned} d_1(t) &= \frac{1}{2}\left[1 + k_1 \cos(\omega t)\right] \\ d_2(t) &= \frac{1}{2}\left[1 + k_2 \cos\left(\omega t - \tfrac{2\pi}{3}\right)\right] \\ d_3(t) &= \frac{1}{2}\left[1 + k_3 \cos\left(\omega t + \tfrac{2\pi}{3}\right)\right] \end{aligned} \tag{15}$$

where $0 \le k_1, k_2, k_3 \le 1$ are the depth of modulation of each modulating function. The modulating functions of (15) correspond to the high-side switches of a bridge inverter. The modulating functions for the low-side switches are the complements of d_1, d_2, and d_3.

The phase voltages generated by the drive are constructed as in (16), which shows that the generated voltages follow the modulating functions with amplitudes proportional to the depth-of-modulation functions k_1, k_2, and k_3. The phase voltages can be written this way under the assumption that the PWM frequency is sufficiently high to ensure that the effects of the inverter switching are filtered completely [11].

$$
\begin{aligned}
v_a &= \frac{1}{2} v_{dc} [d_1 - (1 - d_1)] = \frac{1}{2} v_{dc} (2d_1 - 1) = \frac{k_1}{2} v_{dc} \cos(\omega t) \\
v_b &= \frac{1}{2} v_{dc} [d_2 - (1 - d_2)] = \frac{1}{2} v_{dc} (2d_2 - 1) = \frac{k_2}{2} v_{dc} \cos\left(\omega t - \tfrac{2\pi}{3}\right) \\
v_c &= \frac{1}{2} v_{dc} [d_3 - (1 - d_3)] = \frac{1}{2} v_{dc} (2d_3 - 1) = \frac{k_3}{2} v_{dc} \cos\left(\omega t + \tfrac{2\pi}{3}\right)
\end{aligned} \tag{16}
$$

Since in simulation these voltages are produced directly by the FOC drive, they do not contain the ripple component generated by the input rectifier. However, the ripple can be artificially imposed on the drive phase voltages. Adding ripple to the phase *a* voltage will be considered here; ripple addition to the other two phases is managed in a similar fashion. First, let

$$m_1(t) = k_1 \cos(\omega t)$$

and let the dc bus voltage be split into its average and a ripple component as follows:

$$v_{dc} = \langle v_{dc} \rangle + \tilde{v}_{dc}$$

If the time average of the dc bus voltage is essentially constant when compared with the drive dynamics, the phase *a* voltage generated by the drive can be written as

$$\hat{v}_a = m_1 \frac{\langle v_{dc} \rangle}{2} \tag{17}$$

by definition of the modulating function. The desired result is obtained if we multiply (17) by the dc bus voltage normalized by its average as in (18). This effectively gives the phase voltages as the product of their corresponding modulating functions and the dc bus voltage.

$$\hat{v}_a \frac{v_{dc}}{\langle v_{dc} \rangle} = m_1 \frac{\langle v_{dc} \rangle}{2} \frac{v_{dc}}{\langle v_{dc} \rangle} = m_1 \frac{v_{dc}}{2} \tag{18}$$

This type of construction will impose the necessary rectifier ripple component on the phase voltages generated by the FOC drive. Note that this must be done in the stationary *abc* reference frame, after which the phase voltages are converted back to the synchronous *dq0* reference frame to feed the induction machine model.

Finally, the rectifier LC filter is described by (19), where v_r is the rectifier output voltage, v_{dc} is the filter output voltage, i_L is the rectifier output current, and i_{dc} is the drive dc bus current. The parasitic resistance of the inductor is denoted by R_f.

$$\begin{aligned} L_f \frac{di_L}{dt} &= v_r - v_c - R_f i_L \\ C_f \frac{dv_c}{dt} &= i_L - i_{dc} \end{aligned} \tag{19}$$

The SIMULINK block diagrams of the front-end rectifier and output filter are shown in Figure 3. Interconnection of the FOC controller, dc interface and induction machine is shown in Figure 4. The dc interface is shown in Figure 5.

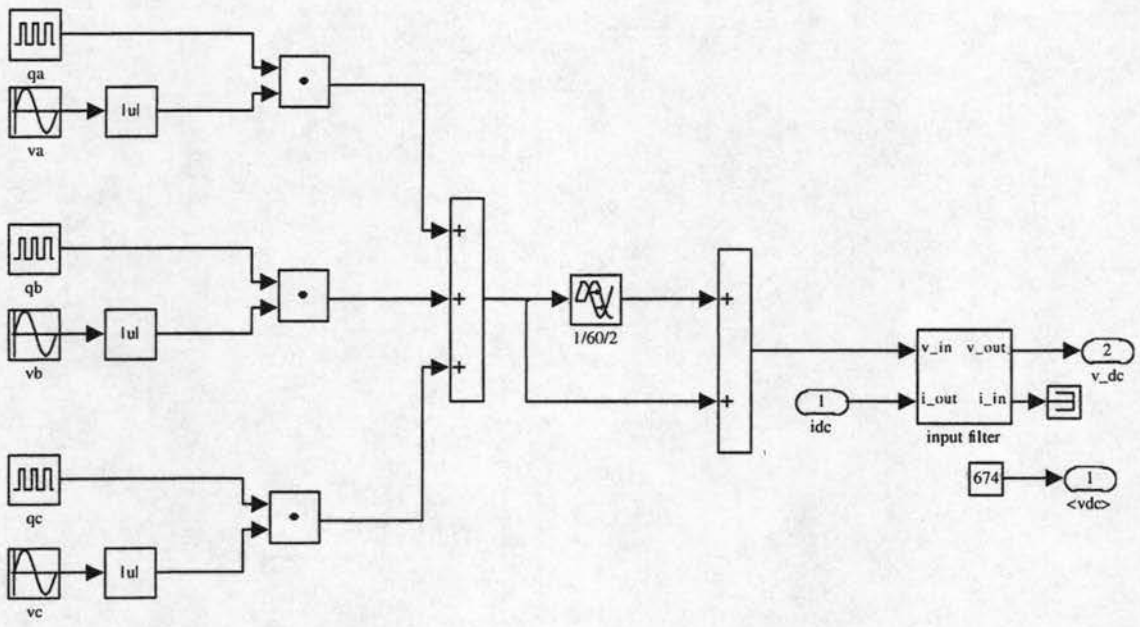

Figure 3: Front-end rectifier and output filter SIMULINK block diagrams.

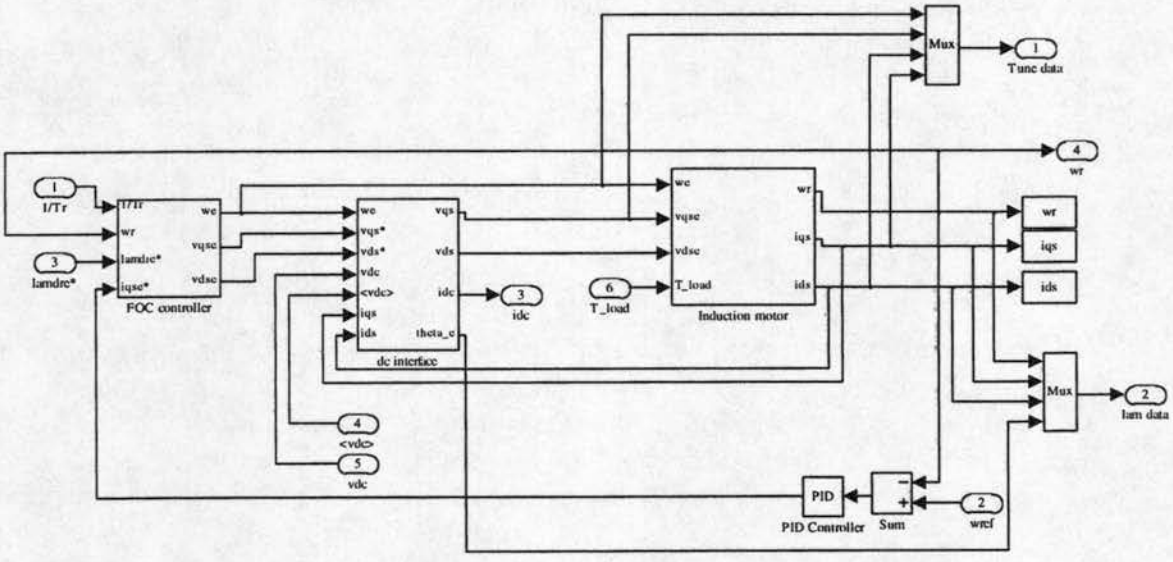

Figure 4: FOC controller, dc interface and induction machine.

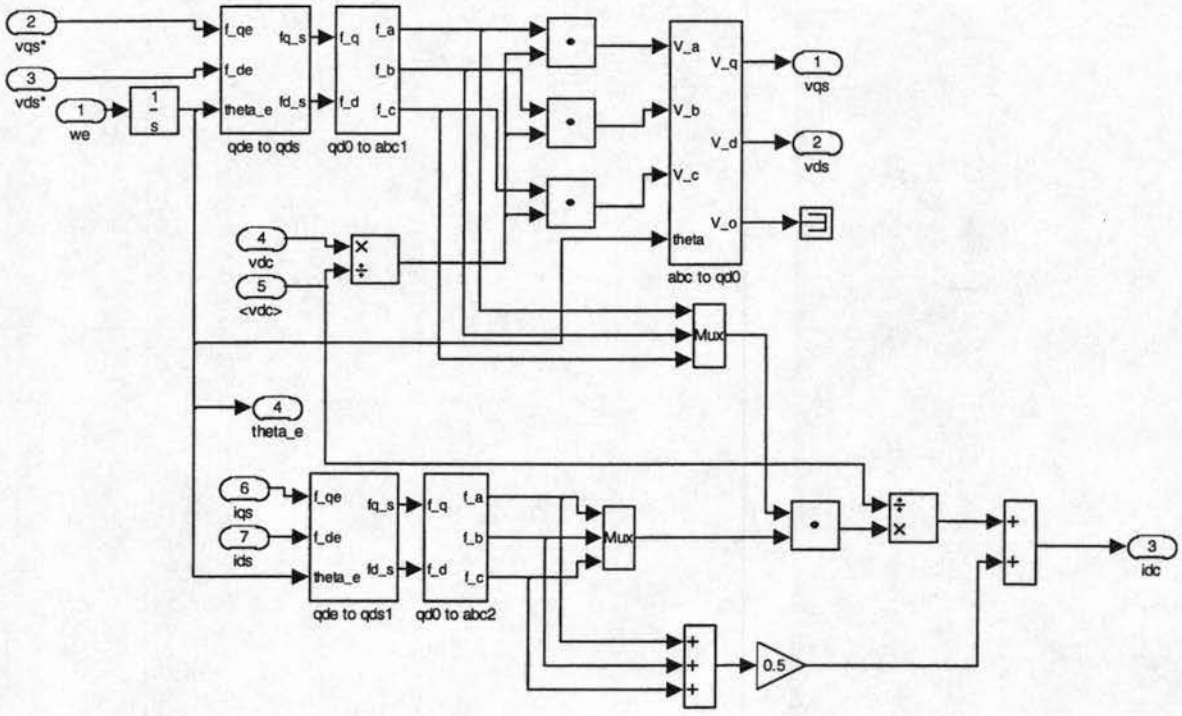

Figure 5: SIMULINK block diagram of the dc interface.

4 PWM Inverter

The electronic drive considered here is an averaged model neglecting the PWM switching transients. The reference voltages created by the FOC controller are assumed to be produced exactly by the inverter [10-12]. The amplitude of the inverter-produced phase voltages is of course limited by the available dc bus voltage. Under this assumption the stator voltages v_{qs} and v_{ds} produced by the FOC control can be directly applied, after the addition of the rectifier ripple, to the induction machine. The only problem concerning the inverter itself that still needs to be solved is the calculation of the dc bus current i_{dc}.

As discussed in the previous section, the three high-side switches of a hex-bridge inverter are controlled with duty ratios $d_1(t)$, $d_2(t)$, and $d_3(t)$. Hence, the dc bus current

can be calculated as the sum of products of the phase currents and the corresponding high-side duty ratio functions as in (20).

$$i_{dc} = d_1 i_a + d_2 i_b + d_3 i_a \tag{20}$$

Note that this calculation is also performed in stationary *abc* coordinates. This is necessary to ensure the proper current ripple components are reflected back to the dc bus. The functions m_1, m_2, and m_3 and, hence, d_1, d_2, and d_3, are not produced directly by the FOC controller. The duty ratio functions can be calculated from the dc bus voltage and the machine phase voltages however. The function m_1 is calculated from (17) as follows:

$$m_1 = \frac{2\hat{v}_a}{\langle v_{dc} \rangle} \tag{21}$$

The other two functions m_2 and m_3 are found in a similar manner. The dc bus current is the given by

$$i_{dc} = \frac{1}{2}\left[1 + \frac{2\hat{v}_a}{\langle v_{dc} \rangle}\right] i_a + \frac{1}{2}\left[1 + \frac{2\hat{v}_b}{\langle v_{dc} \rangle}\right] i_b + \frac{1}{2}\left[1 + \frac{2\hat{v}_c}{\langle v_{dc} \rangle}\right] i_c$$

after simplifying

$$i_{dc} = \frac{1}{2}(i_a + i_b + i_c) + \frac{1}{\langle v_{dc} \rangle}(i_a \hat{v}_a + i_b \hat{v}_b + i_c \hat{v}_c) \tag{22}$$

The first term would not be necessary in a balanced system, but here it is necessary that the current ripple, which does not represent a balanced system, be reflected upon the rectifier output filter.

5 Field-Oriented Controller

The indirect FOC controller for the induction machine is described in this section. The controller is, of course, implemented within the synchronous reference frame. In discussing the design of the FOC controller, it is convenient to look at the induction machine model in terms of flux-linkages and stator and rotor currents [13]. The primes indicating referred rotor quantities have been omitted for simplicity. The derivative operator is denoted by p.

$$v_{qs}^{e} = r_s i_{qs}^{e} + p\lambda_{qs}^{e} + \omega_e \lambda_{ds}^{e} \tag{23}$$

$$v_{ds}^{e} = r_s i_{ds}^{e} + p\lambda_{ds}^{e} - \omega_e \lambda_{qs}^{e} \tag{24}$$

$$0 = r_r i_{qr}^{e} + p\lambda_{qr}^{e} + (\omega_e - \omega_r)\lambda_{dr}^{e} \tag{25}$$

$$0 = r_r i_{dr}^{e} + p\lambda_{dr}^{e} - (\omega_e - \omega_r)\lambda_{qr}^{e} \tag{26}$$

where

$$T_e = \frac{3}{2}\frac{P}{2}\frac{L_m}{L_r}\left(\lambda_{dr}^{e} i_{qs}^{e} - \lambda_{qr}^{e} i_{ds}^{e}\right) \tag{27}$$

$$\lambda_{ds}^{e} = L_{ls} i_{ds}^{e} + L_m\left(i_{ds}^{e} + i_{dr}^{e}\right) \tag{28}$$

$$\lambda_{qs}^{e} = L_{ls} i_{qs}^{e} + L_m\left(i_{qs}^{e} + i_{qr}^{e}\right) \tag{29}$$

$$\lambda_{dr}^{e} = L_{lr} i_{dr}^{e} + L_m\left(i_{ds}^{e} + i_{dr}^{e}\right) \tag{30}$$

$$\lambda_{qr}^{e} = L_{lr} i_{qr}^{e} + L_m\left(i_{qs}^{e} + i_{qr}^{e}\right) \tag{31}$$

Field-oriented control requires that the rotor flux, in the synchronous reference frame, be directed along a single axis, arbitrarily chosen here to be the *d*-axis. Hence, we can write

$$\lambda_{qr}^{e} = 0 \tag{32}$$

Looking at (31), this implies

$$i_{qr}^{e} = -\frac{L_m}{L_m + L_{lr}} i_{qs}^{e} = -\frac{L_m}{L_r} i_{qs}^{e} \tag{33}$$

The values of the control variables must be calculated in the synchronous reference frame and then transformed to the stationary reference frame. The transformation requires knowledge of ω_e. Starting with (25), setting the time derivative of λ_{qr}^{e} to zero, and solving for ω_e-ω_r yields

$$\omega_e - \omega_r = -\frac{r_r i_{qr}^{e}}{\lambda_{dr}^{e}} = s\omega_e \tag{34}$$

The quantity $s\omega_e$ is known as the slip frequency, and is equal to the difference in the synchronous and rotor frequencies. We need the synchronous frequency, which is supplied to the motor model, and its integral, which is used to make the transformation from the synchronous reference frame to the stationary and vice-versa. This is accomplished as follows:

$$\omega_e = \omega_r - \frac{r_r i_{qr}^{e}}{\lambda_{dr}^{e}} \tag{35}$$

$$\theta_e = \int_0^t \omega_e dt \tag{36}$$

Equation (35) represents a problem because the quantity i_{qr}^{e} is not readily accessible. This difficulty can be overcome by substituting (33) into (35) to obtain (37)

$$\omega_e = \omega_r + \frac{r_r}{L_r}\frac{L_m i_{qs}^e}{\lambda_{dr}^e} = \omega_r + \frac{1}{\tau_r}\frac{L_m i_{qs}^e}{\lambda_{dr}^e} \tag{37}$$

where the quantity $\tau_r = L_r / r_r$ is known as the rotor flux time constant.

Since λ_{qr}^{e}=0 under FOC control, from (27) the shaft torque can be written as

$$T_e = \frac{3}{2}\frac{P}{2}\frac{L_m}{L_r}\lambda_{dr}^e i_{qs}^e \tag{38}$$

demonstrating that λ_{dr}^{e} and i_{qs}^{e} are the desired inputs for torque control. If one of these is held constant, direct control over the shaft torque by the other input is achieved. The current i_{qs}^{e} is chosen as the control variable, while the rotor flux is held constant. This results from the delay involved in changing the flux, as shown below.

Since λ_{qr}^{e} is zero under FOC control, (26) can be written as

$$i_{dr}^e = -\frac{1}{r_r} p\lambda_{dr}^e \tag{39}$$

In addition, (30) can be written as

$$\lambda_{dr}^e = L_r i_{dr}^e + L_m i_{ds}^e \tag{40}$$

Now, substitution of (39) into (40) yields

$$\lambda_{dr}^e = \frac{L_m}{1+\tau_r p} i_{ds}^e \tag{41}$$

which shows that changes in i_{qs}^{e} directly affect λ_{dr}^{e}, but with a response governed by the rotor flux time constant. This would not allow instantaneous torque control via the motor

stator currents. However, with the rotor flux constant, the shaft torque can be controlled with no delay via i_{qs}^{e}.

The control variables are i_{qs}^{e} and i_{ds}^{e}, but the actual inputs to the motor are v_{qs}^{e} and v_{ds}^{e}. The FOC controller must calculate these quantities. However, first i_{ds}^{e} must be found. This can be accomplished by rewriting (41) as follows:

$$i_{ds}^{e} = \frac{1}{L_m}(1+\tau_r p)\lambda_{dr}^{e} \tag{42}$$

The stator voltage equations must now be 'decoupled' in order to control the stator currents independently. First solve (30) and (31) for the rotor currents and setting $\lambda_{qr}^{e}=0$. These currents are then substituted into (28) and (29). The resulting stator flux-linkages are substituted into the voltage equations (23) and (24) to give

$$v_{ds}^{e} = (r_s + L_s' p)i_{qs}^{e} + \omega_e\left(L_s' i_{ds}^{e} + \frac{L_m}{L_r}\lambda_{dr}^{e}\right) \tag{43}$$

$$v_{ds}^{e} = (r_s + L_s' p)i_{ds}^{e} - \omega_e L_s' i_{qs}^{e} + \frac{L_m}{L_r} p\lambda_{dr}^{e} \tag{44}$$

where $L_s' = (L_{ls} + L_m) - \frac{L_m^2}{L_r} = L_s - \frac{L_m^2}{L_r}$ is called the stator transient inductance. Equations (43) and (44) can now be used to calculate the required stator voltages using the values of i_{qs}^{e}, i_{ds}^{e}, and λ_{dr}^{e} supplied by the FOC controller. The resulting FOC controller is shown in Figure 6. The slip calculation block utilizes (36) and (37), and the i_{ds}^{e} calculation block uses (42). The voltage decoupling block uses (43) and (44).

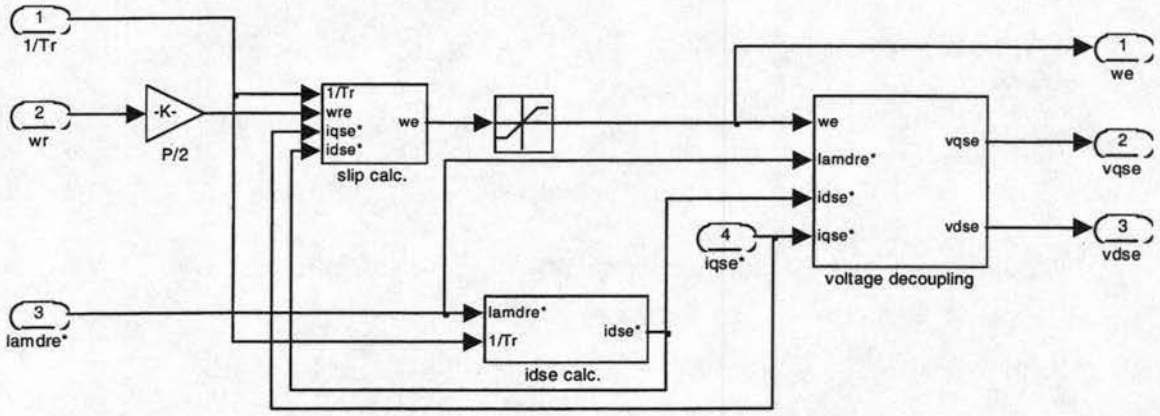

Figure 6: SIMULINK block diagram of FOC controller.

6 Estimation of Rotor Flux Time Constant

The FOC scheme discussed in the previous section requires that machine parameters be known exactly. Although these parameters can be determined to a sufficient degree of accuracy during bench testing, there is a problem if the parameters vary during the course of operation. Of primary interest is the determination of the rotor flux time constant τ_r as the rotor temperature varies. The time constant will vary because the rotor resistance varies with temperature. Variation of the stator resistance is not usually so problematic because this resistance can be estimated through the use of a temperature sensing device or a similar method. Such is not the case with rotor resistance.

When estimating the rotor time constant we assume that when the correct time constant is utilized by the FOC controller, the rotor flux in the synchronous reference frame will be entirely oriented along the *d*-axis [14]. We begin by substituting (28) and (29) into (23) to give

$$v_{qs}^{e} = r_s i_{qs}^{e} + L_s p i_{qs}^{e} + L_m p i_{qr}^{e} + \omega_e L_s i_{ds}^{e} + \omega_e L_m i_{dr}^{e} \tag{45}$$

In steady-state in the synchronous reference frame the currents are constant, and (45) reduces to

$$v_{qs}^{e} = r_s i_{qs}^{e} + \omega_e L_s i_{ds}^{e} + \omega_e L_m i_{dr}^{e} \tag{46}$$

The last term contains the quantity i_{dr}^{e} to which we do not have direct access. However, it can be seen from (39) that

$$\frac{d\lambda_{dr}^{e}}{dt} = 0 \Rightarrow i_{dr}^{e} = 0$$

Therefore, in steady state, we have

$$v_{qs}^{e} - r_s i_{qs}^{e} - \omega_e L_s i_{ds}^{e} = 0 \tag{47}$$

If the rotor flux is not oriented properly, (47) will be non-zero. This property allows (47) to be used to adjust the value of τ_r used by the FOC controller until proper orientation is achieved. This is done by integrating (47) as follows:

$$\hat{\tau}_r = \frac{1}{T_r}\int_0^t \left(v_{qs}^{e} - r_s i_{qs}^{e} - \omega_e L_s i_{ds}^{e}\right) dt \tag{48}$$

where T_r is the estimator time constant, and $\hat{\tau}_r$ is the estimated rotor flux time constant used by the FOC controller.

It is important to note that this estimation scheme is valid only for steady-state operating conditions. However, as will be seen later in simulation, if the load and shaft speed do not vary rapidly, the estimator is satisfactory. The SIMULINK block diagram of the rotor flux time-constant estimator is shown in Figure 7.

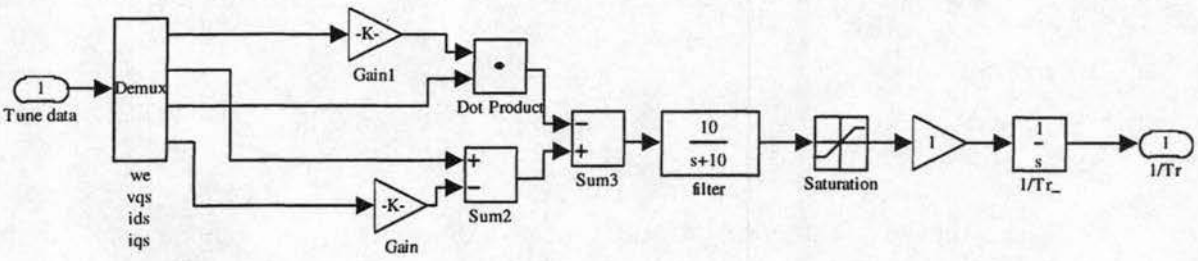

Figure 7: Rotor flux time-constant estimation.

7 Induction Efficiency Optimization

We will now consider the problem of adjusting the reference rotor flux supplied to the FOC drive to optimize operating efficiency. From the torque equation (38), it is apparent there is a continuous set of values for i_{qs}^{e} and λ_{dr}^{e} that will provide a given shaft torque. Efficiency optimization deals with finding the values i_{qs}^{e*} and λ_{dr}^{e*} that provide the desired shaft torque while providing the highest machine operating efficiency. If the drive is set up for speed tracking, then i_{qs}^{e} is derived from the speed error, possibly from a proportional-integral (PI) controller as in (49):

$$i_{qs}^{e} = k_p(\omega_{ref} - \omega_r) + k_i \int_0^t (\omega_{ref} - \omega_r)dt \tag{49}$$

From (49) we see that if the rotor flux is adjusted much more slowly than the speed response, then i_{qs}^{e} will be adjusted so as to maintain the reference torque, and hence the reference speed.

A method for adjusting the rotor flux to maximize efficiency must now be designed. First the rotor flux must be perturbed in some fashion and the resulting change in the input power observed. The rotor and load inertia are large enough to maintain the shaft

speed nearly constant during these perturbations. If the change in rotor flux is positive and results in a negative change in the input power, then the rotor flux reference should be increased in order to increase efficiency. The converse is also true: if the change in rotor flux is positive and the resulting change in the input power is positive, the rotor flux reference should be reduced. The same reasoning applies when the rotor flux perturbation is negative. This is shown in Table 2.

Table 2: Rules for increasing or decreasing λ_{dr}^{e} reference value.

P_{in}	λ_{dr}^{e}	Change in λ_{ref}
$dP_{in}/dt>0$	$d\lambda_{dr}^{e}/dt>0$	Decrease λ_{dr}^{e}
$dP_{in}/dt>0$	$d\lambda_{dr}^{e}/dt<0$	Increase λ_{dr}^{e}
$dP_{in}/dt<0$	$d\lambda_{dr}^{e}/dt>0$	Increase λ_{dr}^{e}
$dP_{in}/dt<0$	$d\lambda_{dr}^{e}/dt<0$	Decrease λ_{dr}^{e}

The description above indicates that we are looking for a correlation between the dc bus power and the rotor flux. Table 2 shows that a convenient way of adjusting the rotor flux is to use the correlation between the rotor flux and input power as an error signal for optimizing the machine operating efficiency. Let the reference rotor flux be given by [3,15]

$$\lambda_{ref} = -T_{flux}\int_{0}^{t}\left(\frac{dP_{in}}{dt}\frac{d\lambda_{dr}^{e}}{dt}\right)dt \tag{50}$$

Note that this integral will correctly produce the necessary changes in λ_{ref} given by Table 2. However, the derivatives will also capture the change in rotor flux and input power due to the control action, not just the perturbations introduced by the rectifier. This is not a

problem if the control action is 'slow-acting' as compared with perturbation frequency. The derivatives due to the control action will be very small.

Using the control law, the rotor flux is effectively adjusted until optimal operating efficiency is achieved. Convergence to the optimal flux value can be improved by taking into account the delay between the perturbation of machine phase voltages and the resulting rotor flux change. Perturbations in the input voltage that introduce changes in the input power do not immediately affect the rotor flux. The inverter input power is affected because the dc bus voltage contains the rectifier output ripple component. However, there is a delay between the perturbations in the input voltage and those in the rotor flux.

To solve for this delay characteristic, start with (26) and solve for the *d*-axis rotor current in the rotor reference frame as in (51):

$$i_{dr}^{r} = -\frac{1}{r_r} p\lambda_{dr}^{r} \tag{51}$$

Substitute this result into (30) and solve $\lambda_{dr}{}^{e}$ to obtain

$$\lambda_{dr}^{r} = \frac{L_m}{1+\frac{L_r}{r_r} p} i_{ds}^{r} \tag{52}$$

Equation (52) shows that changes in the stator currents are transferred to the rotor flux with time constant equal to the rotor flux time constant τ_r. Of course, the perturbations are introduced in the stator voltages, but the drive input power and not the machine voltages is being correlated with the rotor flux. The rotor flux time constant is provided by the estimator described above.

One problem remains: calculation of the rotor flux in the synchronous frame *d*-axis. Start by solving (25) and (26) for the rotor current components in the rotor reference frame as follows:

$$i_{qr}^{r} = -\frac{1}{r_r} p\lambda_{qr}^{r} \tag{53}$$

$$i_{dr}^{r} = -\frac{1}{r_r} p\lambda_{dr}^{r} \tag{54}$$

Substitute these two equations into (30) and (31) to yield

$$\lambda_{qr}^{r} = \frac{L_m}{1+\frac{L_r}{r_r} p} i_{qs}^{r} \tag{55}$$

$$\lambda_{dr}^{r} = \frac{L_m}{1+\frac{L_r}{r_r} p} i_{ds}^{r} \tag{56}$$

Equation (56) gives the *d*-axis rotor flux in the rotor reference frame. It is required to solve for both rotor components in order to make the transformation from the rotor frame back to the synchronous frame. The assumption that the *q*-axis rotor flux is zero is not valid even under FOC control. The FOC controller is not capable of regulating the perturbations in the rotor flux. Again, the rotor flux time constant is supplied by the estimator. The SIMULINK block diagram of the efficiency optimizer is shown in Figure 8.

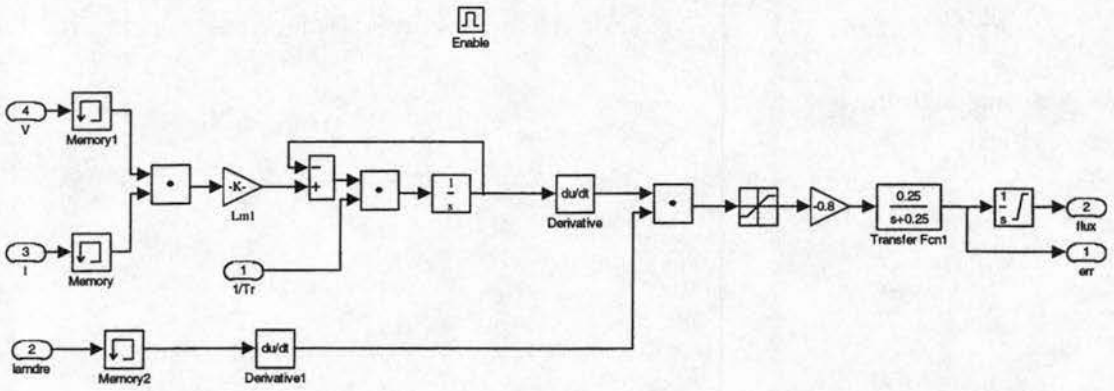

Figure 8: SIMULINK block diagram of efficiency optimizer.

8 Simulation Examples

Section 8 will present simulation examples of the systems described above. Example 1 shows the operation of the induction machine under FOC control. The motor and rectifier parameters are given in Table 3. For the first simulation, the induction machine is initially loaded at 5 N·m with the reference speed held at zero. At time equal to 1 s the reference speed is brought to –100 rad/s, and then to +100 rad/s at 4 s. At time equal to 7 s the load is brought to 35 N·m. The reference speed and shaft speed are shown in Figure 9. The FOC controller provides excellent speed tracking and load disturbance rejection.

Table 3: Motor and rectifier parameters.

Parameter	Value
Average rectifier output voltage	674 V
Filter inductance	100 μH
Filter capacitance	1000 μF
Induction machine poles	4
Magnetizing inductance	5.5 mH
Stator leakage inductance	400 μH
Rotor leakage inductance	400 μH
Stator series resistance	0.25 Ω
Rotor series resistance	0.25 Ω
Base frequency	200 rad/s
Induction machine inertia	0.01 kg·m^2

The stator currents components are shown in Figure 10. Note that the *d*-axis current is constant. This is expected because the *d*-axis rotor current is held constant. The *q*-axis current provides the necessary shaft torque to sustain the load. The rectifier ripple components are easy to distinguish on the current waveforms.

The rotor flux components are displayed Figure 11. The *d*-axis component is brought up to the reference value and held. The *q*-axis component is brought to zero and remains there with slight transients as the reference speed or the load torque are changed abruptly. Again, the ripple imposed by the rectifier is readily apparent.

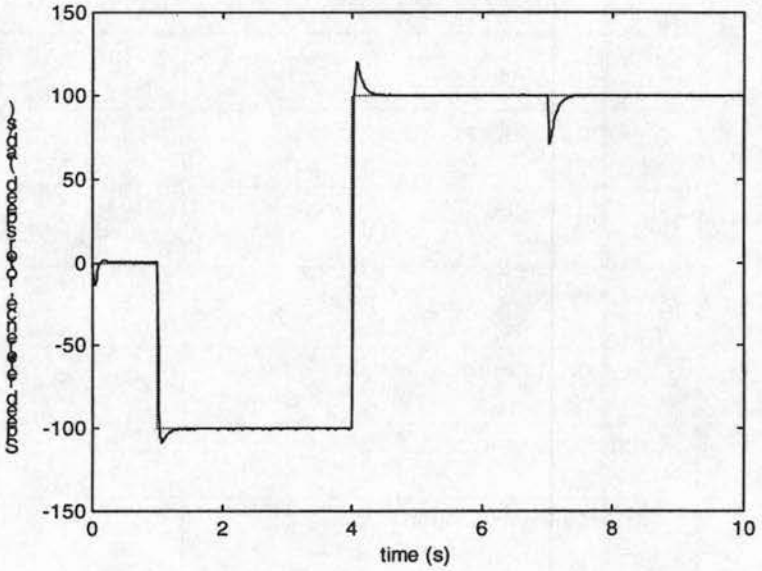

Figure 9: Induction motor reference speed and shaft speed.

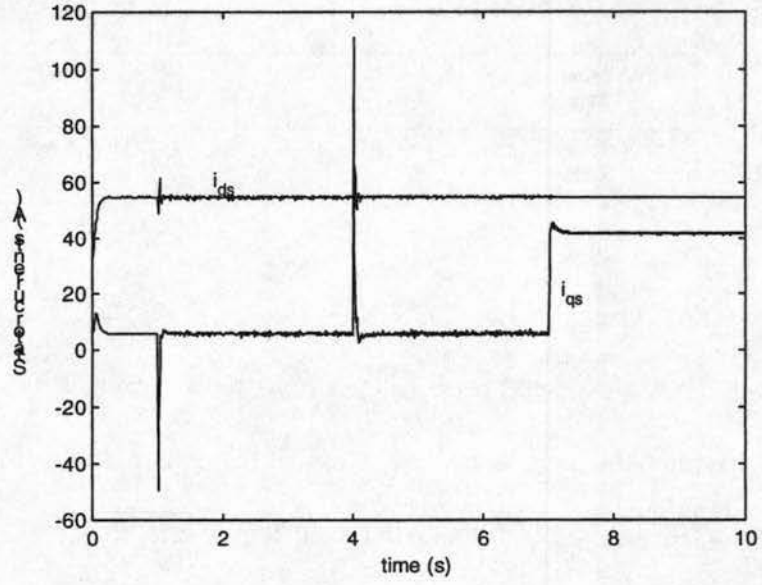

Figure 10: Induction machine stator currents in synchronous reference frame.

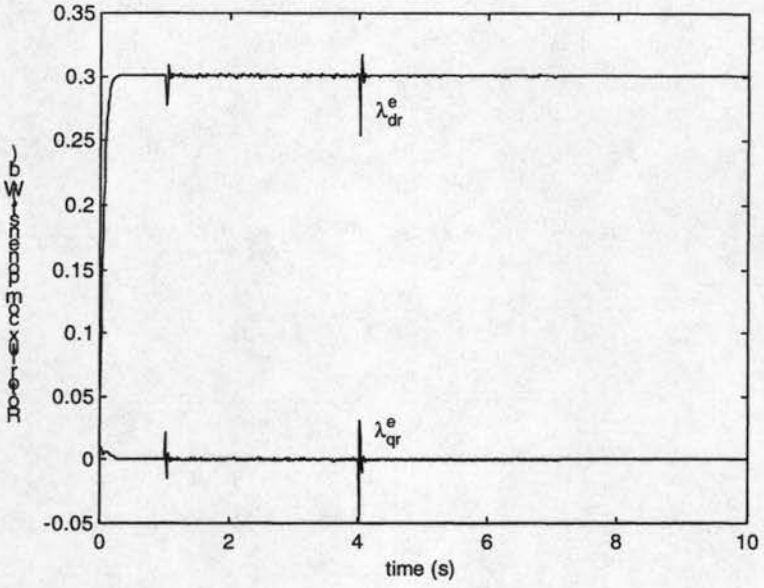

Figure 11: Rotor flux components in synchronous reference frame.

Finally, Figure 12 shows the dc bus voltage and current. The bus voltage is almost constant while the current varies with the current demand imposed by the inverter. The rectifier ripple is present in both waveforms.

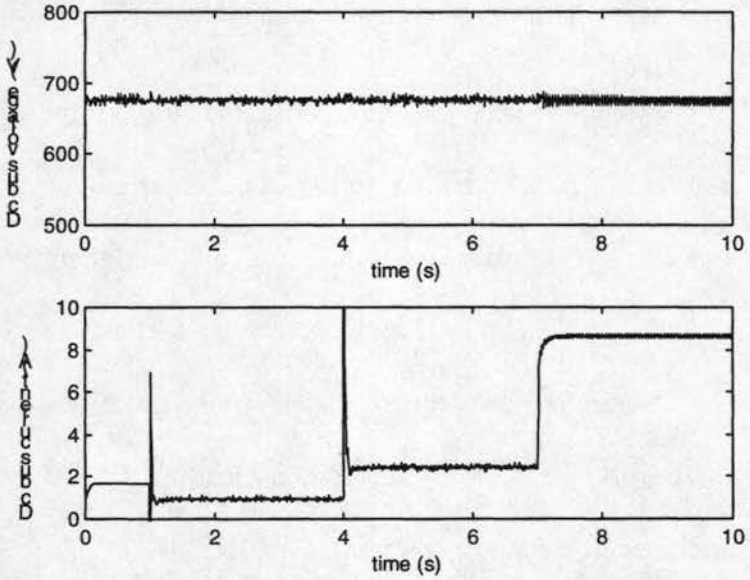

Figure 12: Dc bus voltage and current.

Example 2 includes all of the components presented above including rotor time-constant estimation and efficiency optimization. The reference speed is brought to 100 rad/s at 1 s and increased to 135 rad/s at 75 s. The shaft load is initially 5 N·m and increased to 35 N·m at 1 s, and again to 55 N·m at 40 s. The machine speed and load torque are shown in Figure 13.

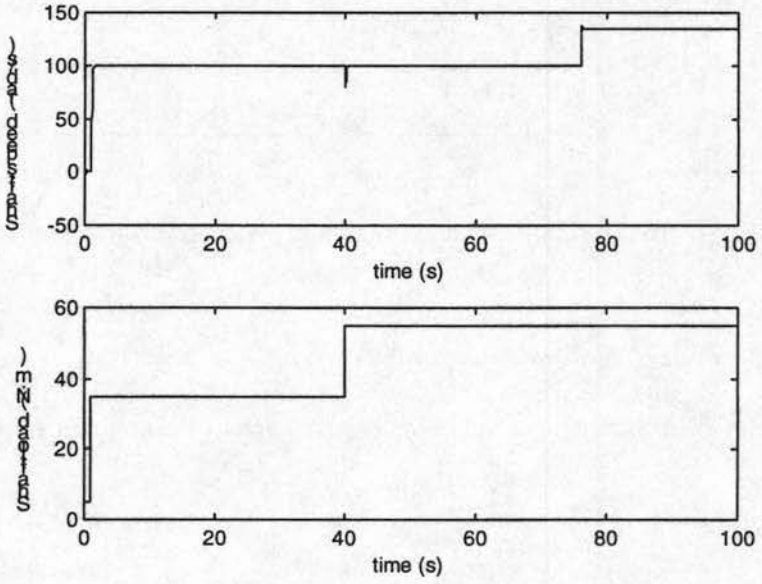

Figure 13: Induction motor shaft speed and load.

The operating efficiency optimization of the induction machine is shown in Figure 14. The *d*-axis rotor flux is varied according to the correlation between the derivative of the dc bus power and the derivative of the rotor flux. The figure shows how, at startup, and after changes in speed and load torque, the flux is adjusted and the efficiency rises to its maximum. The optimization time constant is on the order of 20 s. A faster response can be achieved at the expense of having additional overshoot. Note that the optimization is more critical when the motor is lightly loaded.

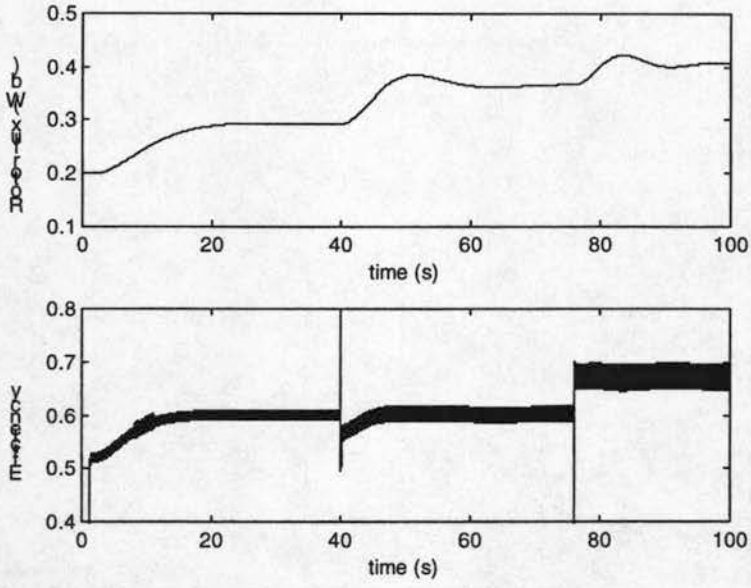

Figure 14: Rotor flux in synchronous reference frame and overall efficiency.

The estimation of the reciprocal of the rotor flux time constant is shown in Figure 15. The lock-in time is on the order of 30 s. Also, note that the estimator has to recover after every transient, since the estimator equation is based on a steady state analysis. However, the error is not large enough to cause any problems with the FOC controller or the optimization process. In a real application, the response of the optimization process and the rotor time-constant estimation should have a wider time scale separation in order to prevent oscillation in either rotor flux reference or the time constant estimate. In other words, the two are dependent processes.

The stator currents in the synchronous reference frame are shown in Figure 16. The dc bus voltage and current are shown in Figure 17, and the dc bus power to the inverter is shown in Figure 18. Note that since the shaft speed of the induction machine is regulated that the inverter input power is inversely proportional to the efficiency.

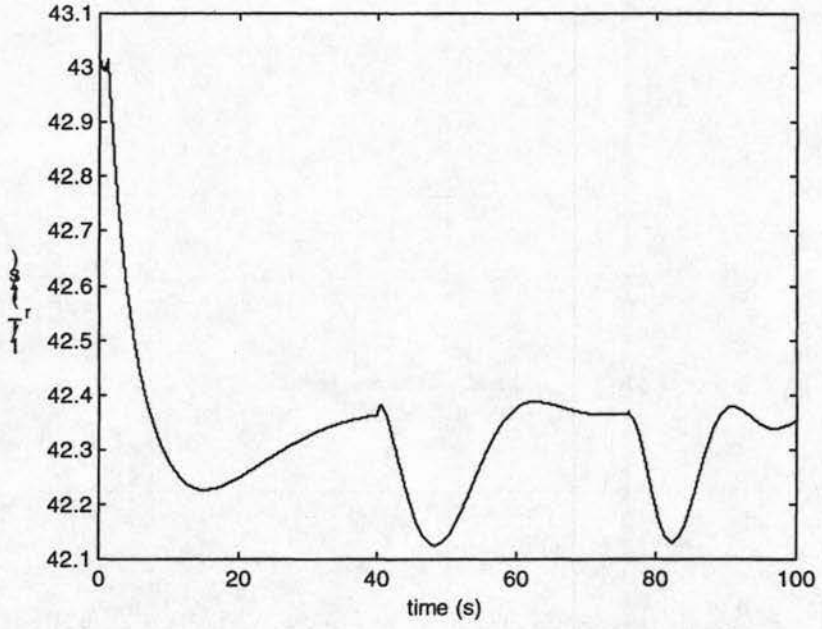

Figure 15: Estimation of reciprocal of the rotor flux time constant.

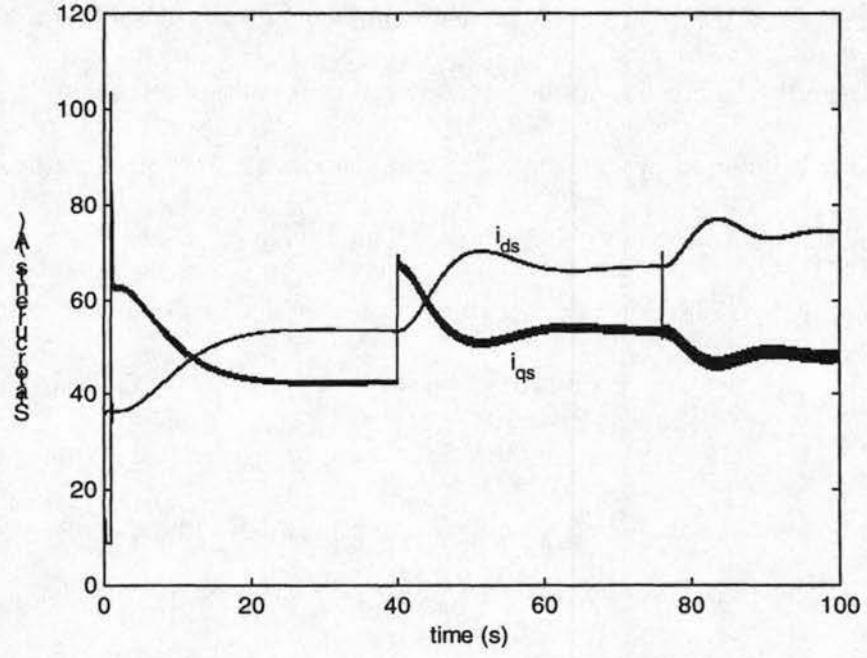

Figure 16: Stator currents in synchronous reference frame.

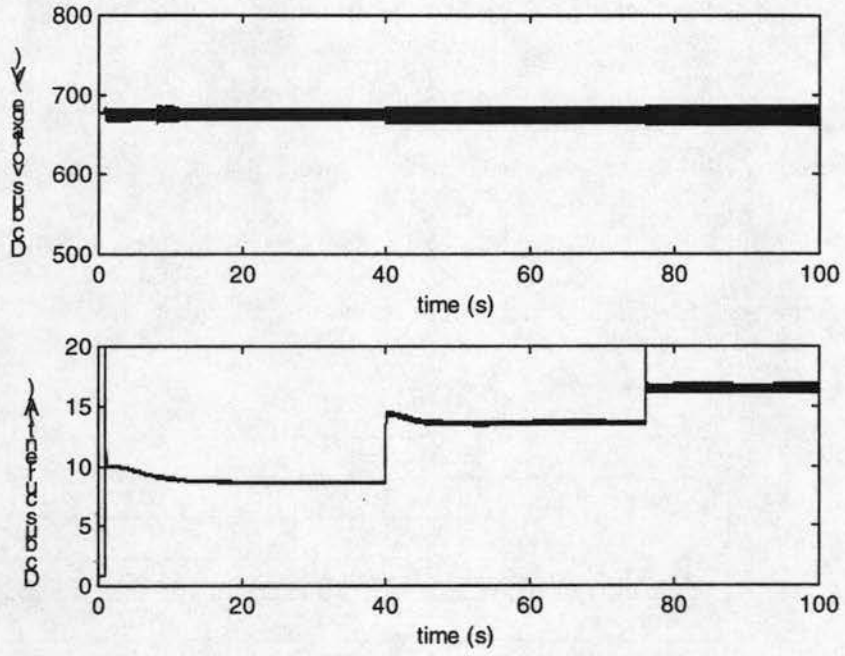

Figure 17: Dc bus voltage and current.

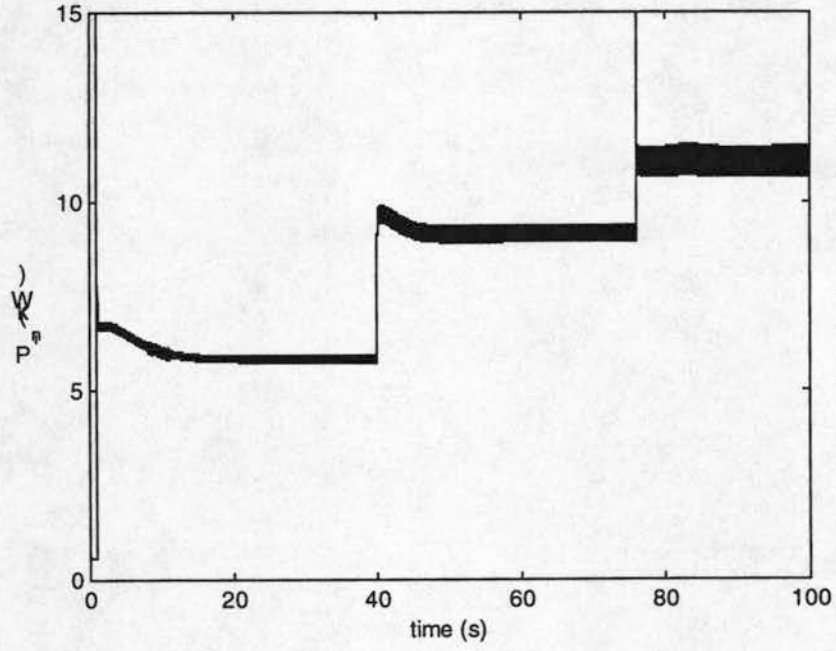

Figure 18: Dc bus power to inverter.

9 Induction Motor Efficiency Optimization

In section 9 comparison is made between a conventional FOC-controlled induction machine with a constant rotor flux reference, and the same system with rotor flux optimization. The machine model used takes into account saturation of the magnetizing inductance. The induction machine parameters are given in Table 4.

Table 4: Induction machine parameters.

Parameter	Value
Number of poles	4
Stator leakage inductance	400 μH
Rotor leakage inductance (referred)	400 μH
Stator series resistance	0.25 Ω
Rotor series resistance (referred)	0.25 Ω
Magnetizing inductance	5.5 mH
Continuous rated power	20 HP

Saturation in the induction machine is handled by directly changing the magnetizing inductance L_m as follows:

$$L_m = f_m\left(\lambda_m^e\right) \tag{57}$$

where

$$\lambda_m^e = \sqrt{\left(\lambda_{mq}^e\right)^2 + \left(\lambda_{md}^e\right)^2} \tag{58}$$

This is the equivalent of changing μ in the main flux path of the induction machine. The scaling of the nominal value of L_m with $\lambda_m{}^e$ is shown in Figure 19:

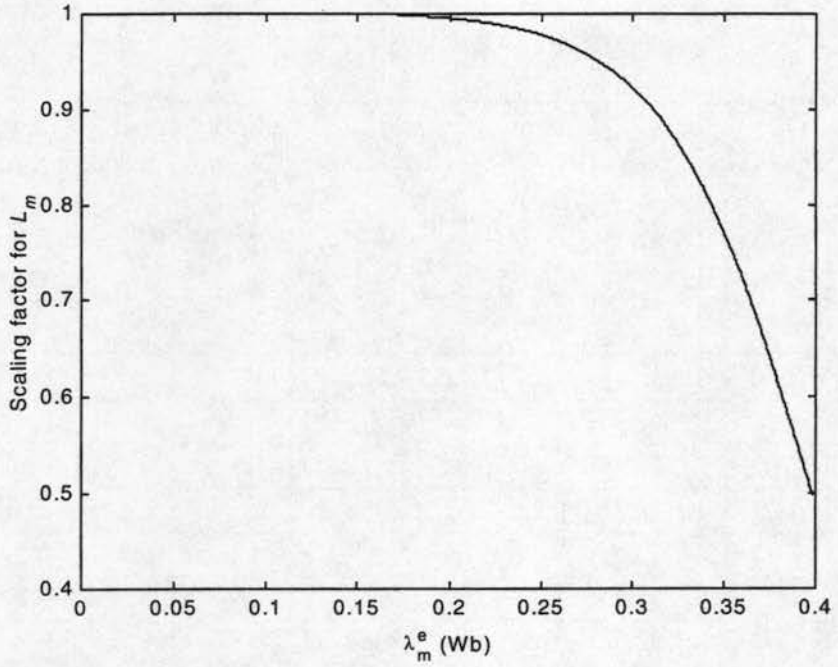

Figure 19: Scaling of magnetizing inductance with $\lambda_m{}^e$.

Table 5 shows the comparison between the conventional FOC controlled induction machine and the optimized version. The shaft speed is regulated at 200 rad/s. As expected, for light loads the operating efficiency increases significantly with a reduction in field excitation. As the load is increased near rated torque, the conventional setup efficiency is equal to the efficiency of the optimized setup. A plot of the operating efficiencies vs. load torque for both setups is shown in Figure 20.

Table 5: Comparison of conventional and optimized FOC-controlled induction machine.

Load torque (N.m)	Output power (W)	$\eta_{conventional}$ (%) (λ_{dr}^{e}=0.45 Wb)	Input power (Fixed λ_{dr}^{e})	$\eta_{optimized}$ (%)	Intput power (optimized	λ_{dr}^{e} (Wb) (optimized)
10	2000	8.77	22805	69.00	2899	0.250
20	4000	17.54	22805	73.10	5472	0.271
35	7000	25.44	27516	70.76	9893	0.325
55	11000	40.35	27261	61.99	17745	0.38
75	15000	48.54	30902	66.96	22401	0.369
90	18000	51.75	34783	66.67	26999	0.361
105	21000	52.92	39683	54.09	38824	0.446
110	22000	52.92	41572	53.51	41114	0.45
125	25000	52.05	48031	51.46	48581	0.461

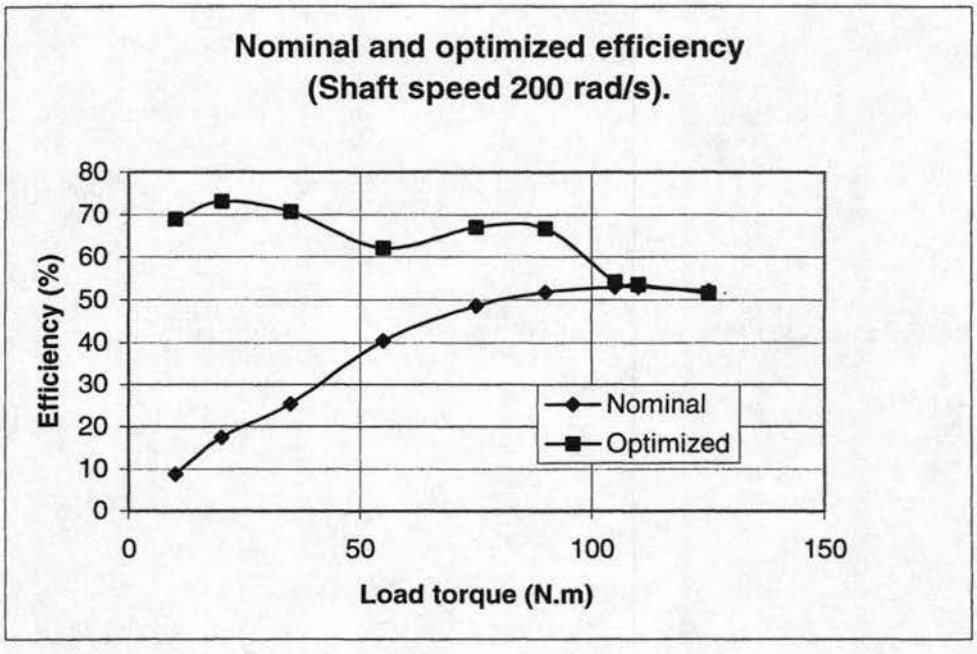

Figure 20: Operating efficiency of conventional and optimized FOC-controlled induction machine.

For this motor, a load of about 93 N·m corresponds to rated load. Fig. 20 confirms that efficiency improvements are substantial at all load levels below the rated value. Table 5 confirms that loss is reduced considerably. The 1% increase in loss at 125 N-m load shows the residual error of the observer when the magnetics are well into saturation, but even in this case the system was able to reach within about 1% of the lowest loss operating point. The Table 5 results also confirm that efficiency improvements are considerable over a wide load range, and not just for highly underloaded situations. At 35 N-m (about 38% of rated load), for example, the optimizing control saves 17.6 kW – nearly as much as the rated motor output power. Efficiency improves as the load reduces, most likely because extra losses from high magenetic saturation currents are lower at low flux.

10 Conclusion

The modeling and simulation of an FOC-controlled three-phase induction machine has been presented. In addition, a method of estimation of the rotor flux time constant has been provided. The estimated time constant is utilized by the FOC controller and an operating ripple-correlation efficiency optimizer. Maximization of the operating efficiency of the induction machine is effected by examining the cross-correlation between the inverter input power ripple and the rotor flux ripple, and then adjusting the rotor flux to null out this correlation.

In contrast to the use of ripple control for solar power processing, motor systems require compensation for reactive effects to ensure correct convergence of the control. It was demonstrated that ripple correlation can be applied successfully when an observer is employed to support the necessary reactive compensation. Simulation studies were used

to evaluate controller performance, in the presence of magnetic saturation. Results for a sample test motor revealed substantial reductions in power loss when ripple correlation control is applied. The method of ripple correlation control shows great promise for reducing the energy usage of electronic motor drive systems.

11 References

[1] P. Midya, P. T. Krein, R. J. Turnbull, R. Reppa, J. Kimball, "Dynamic maximum power point tracker for photovoltaic applications," in *Rec., IEEE Power Electronics Spec. Conf.,* 1996, pp. 1710-1716.

[2] P. Midya, P. T. Krein, R. J. Turnbull, "Self-excited power minimizer/maximizer for switching power converters and switching motor drive applications," United States Patent 5,801,519, Sep. 1, 1998.

[3] P. T. Krein, "Ripple correlation control, with some applications," *ISCAS*, Vol. 5, 1999, pp. 283-286.

[4] S. M. Meerkov, "Principle of vibrational control: theory and applications," *IEEE Trans. Automatic Control*, vol. AC-25, pp. 755-762, 1980.

[5] C. R. Sullivan, M. J. Powers, "A high-efficiency maximum power point tracker for photovoltaic arrays in a solar-powered race vehicle," in *Rec., IEEE Power Electronics Spec. Conf.,* 1993, pp. 574-580.

[6] J. H. R. Enslin, D. B. Snyman, "Combined low-cost high-efficient inverter, peak power tracker and regulator for PV applications," *IEEE Trans. Power Electronics*, Vol. 6, no. 1, pp. 73-82, 1991.

[7] P. Famouri, J. J. Cathey, "Loss minimization control of an induction motor drive," *IEEE Trans. Industry Applications*, Vol. 27, no. 1, pp. 32-47, 1991.

[8] P. C. Krause, O. Wasynczuk, S. D. Sudhoff, *Analysis of Electric Machinery*. New York, NY: IEEE, 1995.

[9] C. Ong, *Dynamic Simulation of Electric Machinery Using MATLAB/SIMULINK*. Upper Saddle River, NJ: Prentice Hall, 1998.

[10] P. T. Krein, *Elements of Power Electronics*. New York: Oxford University Press, Inc., 1998.

[11] P. T. Krein, J. Bentsman, R. M. Bass, B. L. Lesieutre, "On the use of averaging for the analysis of power electronic systems," *IEEE Trans. Power Electronics*, Vol. 5, no. 2, pp. 182-190, 1990.

[12] J. G. Kassakian, M. F. Schlecht, G. C. Verghese, *Principles of Power Electronics*. New York: Addison-Wesley Publishing Company, Inc., 1991.

[13] D. W. Novotny and T. A. Lipo, *Vector Control and Dynamics of AC Drives*. New York: Oxford Press Inc., 1996.

[14] W. Leonhard, *Control of Electrical Drives*. New York: Springer-Verlag, 1996.

[15] R. S. Reppa, "A maximum power point tracker for photovoltaic applications," University of Illinois, Master's Thesis, Tech. Rep. PAP-TR-96-3, May 1996.